AIAA 80-0067R

Two-Dimensional Inlet Simulation Using a Diagonal Implicit Algorithm

D. S. Chaussee*
Flow Simulations, Inc., Sunnyvale, Calif.
and
T. H. Pulliam†
NASA Ames Research Center, Moffett Field, Calif.

A modification of an implicit approximate-factorization finite-difference algorithm applied to the two-dimensional Euler and Navier-Stokes equations in general curvilinear coordinates is presented for supersonic freestream flow about and through inlets. The modification transforms the coupled system of equations into an uncoupled diagonal form which requires less computation work. For steady-state applications the resulting diagonal algorithm retains the stability and accuracy characteristics of the original algorithm. Solutions are given for inviscid and laminar flow about a two-dimensional wedge inlet configuration. Comparisons are made between computed results and exact theory.

Nomenclature

$\bar{a},\bar{b}$ = constants defined in Eq. (8a)
A,B = matrices defined in Eq. (10b)
$\hat{A},\hat{B}$ = Jacobian matrices defined in Eq. (10a)
c = local speed of sound
D = diagonal matrix defined in Eq. (12b)
e = total energy per unit volume defined in Eq. (2)
E,F = vector arrays defined in Eq. (1)
$\hat{E},\hat{F}$ = vector arrays defined in Eq. (5)
f_1,f_2,f_3 = defined in Eq. (8b)
h = time step = Δt or $\Delta t/2$
I = identity matrix
J = Jacobian of transformation
$\bar{k}_x,\bar{k}_y$ = k_x or $k_y/(k_x^2+k_y^2)$
m_1,m_2 = defined in Eqs. (13)
m_{21},m_{31},m_{41}, m_{42},m_{43},m_{44} = defined in Eqs. (16b)
$\hat{M}$ = viscous matrix defined in Eqs. (16a) and (16b)
N = $T_\xi^{-1}T_\eta$
$\hat{N}_j$ = matrix defined in Eq. (13)
p = dimensionless pressure, $\bar{p}/\gamma p_\infty$
Pr = Prandtl number
$q,\hat{q}$ = vector arrays defined in Eq. (1)
Re = Reynolds number
$\hat{R}$ = right-hand side matrix defined in Eq. (11)
$\hat{S}_\eta$ = viscous matrix defined in Eq. (15)
t = dimensionless time in physical space
$T_k = T_k^{-1} = \xi,\eta$ = matrices defined in Eq. (12c)
u,v = Cartesian velocity component in x and y directions, respectively
U,V = contravariant velocities defined in Eq. (4)
x,y = physical coordinates
x_t,x_ξ,x_η; y_t,y_ξ,y_η = geometric derivatives
α = $\rho/(\sqrt{2}c)$
$\alpha_1,\alpha_2,\alpha_3,\alpha_4$ = defined in Eqs. (16b)
β = $1/(\sqrt{2}c\rho)$
γ = ratio of specific heat
$\delta_\delta,\delta_\eta$ = central difference operators
Δt = time step = h
Δ_ξ,Δ_η = backward difference operators
ϵ_I = implicit smoothing, usually $2^*\epsilon_E$
ϵ_E = explicit smoothing, usually = h
η = generalized coordinate normal to body
η_t,η_x,η_y = metrics defined in Eq. (3)
$\bar{\theta}$ = defined as $\bar{k}_x u+\bar{k}_y v$
κ = coefficient of heat transfer
Λ_ξ,Λ_η = matrices defined in Eq. (12b)
μ = $1/\sqrt{2}$, or coefficient of viscosity
ξ = generalized coordinate parallel to body
ξ_t,ξ_x,ξ_y = metrics defined in Eq. (3)
ρ = dimensionless density, $\bar{\rho}/\rho_\infty$
τ = dimensionless time in transformed space
ϕ^2 = defined as $0.5(\gamma-1)(u^2+v^2)$
∇_ξ,∇_η = forward difference operators

Presented as Paper 80-0067 at the AIAA 18th Aerospace Sciences Meeting, Pasadena, Calif., Jan. 14-16, 1980; submitted Feb. 7, 1980; revision received Aug. 5, 1980.

*Senior Research Scientist. Member AIAA.
†Research Scientist. Member AIAA.

Introduction

PROPER design of the air inlets is a crucial factor in achieving the desired performance of supersonic airbreathing missiles and aircraft. In the typical inlet design case, mass flow adequate to the demands of the propulsion system with maximum total pressure recovery and minimum external drag is required for a range of freestream conditions and vehicle altitudes. Meeting these requirements has traditionally required extensive experimental development. Recent trends indicate, however, that certain features of the complicated inlet flowfield are amendable to computation, even though existing methods have some shortcomings. Rizzi and Schmidt[1] have applied a finite-volume approach to low-supersonic inlet flowfields with reasonable success. Arlinger[2] and Reyhner[3] have developed numerical methods that are based on the full-potential equation. Adoption of the full-potential equation for supersonic flow above a Mach number of 1.3 should be avoided, however, due to the difference in shock jump conditions used from the exact shock jump conditions; this procedure also disregards the total pressure loss in the inlet which is very critical in supersonic inlet design. Bansod[4] and Hawkins et al.[5] have applied explicit numerical methods to transonic flow about inlets. These methods,

however, even if extended to the supersonic regime, would be limited in convergence rate due to the necessary clustering of points near the cowl lip which reduces the integration step size. More recently the first author has developed a method[6] which is implicit in nature and faster than the previous methods. Other available methods[7,8] are for supersonic internal flows.

This paper describes a new method of calculating the flowfield around and through two-dimensional inlets that does not have the limited Mach number range of potential methods; that is considerably faster than the methods of Refs. 4-6; and that is valid for subcritical, critical, and supercritical mass flow rates. In the present method,[9] a modification of an implicit approximate-factorization finite-difference algorithm[10,11] applied to partial differential equations is presented which substantially reduces the total computation work. The modification takes the coupled system of equations into an uncoupled diagonal form which is easier to solve. The resulting diagonal algorithm retains the stability and many of the accuracy characteristics of the original algorithm. Since the governing equations written in generalized coordinates are cast in conservation law form, the complex features of the inlet flowfield are captured correctly. With the equations cast in generalized coordinates, mesh-generating routines[12,13] are used to create the computational mesh. Clustering of grid points near solid surfaces is allowed. The implicit algorithm is then used to advance the unsteady equations in time with the ability of being able to take larger time steps than the previous explicit techniques, thus allowing faster convergence.

Several different types of boundary conditions are required. At solid boundaries, the tangency condition is incorporated as no flow through the boundary or a no-slip condition for the viscous cases. The upstream and lateral boundaries are specified so that freestream conditions may be specified (and these may be nonuniform). At outflow, if the flow is purely supersonic the variable are extrapolated. If the outflow is subsonic, as in a critical or subcritical calculation, the back pressure is specified and all other variables are calculated from characteristic-like equations of Kentzer.[14]

Governing Equations

The partial differential equations governing the two-dimensional planar flow of an unsteady inviscid, nonheat-conducting, ideal gas can be written in nondimensional strong conservation law form[15] under the generalized independent variable transformation

$$\tau=t, \quad \xi=\xi(t,x,y), \quad \eta=\eta(t,x,y)$$

as follows:

$$\hat{q}_\tau+[(\xi_t q+\xi_x E+\xi_y F)/J]_\xi+[\eta_t q+\eta_x E+\eta_y F)/J]_\eta=0 \quad (1)$$

where

$$\hat{q}=J^{-1}\begin{bmatrix}\rho\\ \rho u\\ \rho v\\ e\end{bmatrix} \quad E=\begin{bmatrix}\rho v\\ \rho u^2+p\\ \rho uv\\ (e+p)u\end{bmatrix} \quad F=\begin{bmatrix}\rho v\\ \rho uv\\ \rho v^2+p\\ (e+p)v\end{bmatrix}$$

and the Jacobian

$$J=\xi_x\eta_y-\xi_y\eta_x$$

In Eq. (1), p represents the pressure, ρ the density, u and v the velocity components in the x and y directions, respectively, and e the total energy per unit volume. The following equation relates the pressure, density, and velocity components to the energy for an ideal gas

$$e=p/(\gamma-1)+\rho(u^2+v^2)/2 \quad (2)$$

Equation (1) was integrated forward in time to a steady-state condition using an existing implicit Euler equation solver.[11]

The metrics in Eq. (1), ξ_t, ξ_x, etc., are easily formed from the derivatives of x_τ, x_ξ, etc., using the relations

$$\xi_x=Jy_\eta, \quad \xi_y=-Jx_\eta, \quad \xi_t=-x_\tau\xi_x-y_\tau\xi_y$$

$$\eta_x=-Jy_\xi, \quad \eta_y=Jx_\xi, \quad \eta_t=-x_\tau\eta_x-y_\tau\eta_y \quad (3)$$

It is also convenient to define the velocities

$$U=\xi_t+\xi_x u+\xi_y v$$

$$V=\eta_t+\eta_x u+\eta_y v \quad (4)$$

which are the so-called contravariant velocities along the ξ and η coordinates. Using these defined velocities, $\hat{E}$ and $\hat{F}$ can be written in the compact form

$$\hat{E}=J^{-1}\begin{bmatrix}\rho U\\ \rho uU+\xi_x p\\ \rho vU+\xi_y p\\ (e+p)U-\xi_t p\end{bmatrix} \quad \hat{F}=J^{-1}\begin{bmatrix}\rho V\\ \rho uV+\eta_x p\\ \rho vV+\eta_y p\\ (e+p)V-\eta_t p\end{bmatrix} \quad (5)$$

Note that once U and V are formed, the flux vectors $\hat{E}$ and $\hat{F}$ are not much more complex than E and F. To complete the problem, boundary and initial conditions must be specified.

Boundary Conditions

Along the body surface $\eta(x,y,t)=0$ (the cowl, ramp, and inlet surfaces of Fig. 1), the condition of tangency in unsteady flow is enforced by

$$V=0 \text{ with } \begin{pmatrix}u\\ v\end{pmatrix}=J^{-1}\begin{bmatrix}\eta_y & -\xi_y\\ -\eta_x & \xi_x\end{bmatrix}\begin{pmatrix}U-\xi_t\\ -\eta_t\end{pmatrix} \quad (6)$$

For viscous flow, $U=0$ is used in Eq. (6) to produce no-slip conditions.

The pressure on the body surface can be obtained from the normal momentum equation

$$\rho[\partial_\tau\eta_t+u\partial_\tau\eta_x+v\partial_\tau\eta_y]-\rho U(\eta_x u_\xi+\eta_y v_\xi)$$

$$=(\eta_x\xi_x+\xi_y\eta_y)p_\xi+(\eta_x^2+\eta_y^2)p_\eta=J^{-1}\sqrt{\eta_x^2+\eta_y^2}\,p_n \quad (7)$$

where n is the direction normal to the body surface.

At the internal outflow plane there are two possible flow conditions. If the flow is supersonic, the conservative variables are zero-order extrapolated; whereas if the flow is subsonic, the back pressure is specified and Kentzer's[14]

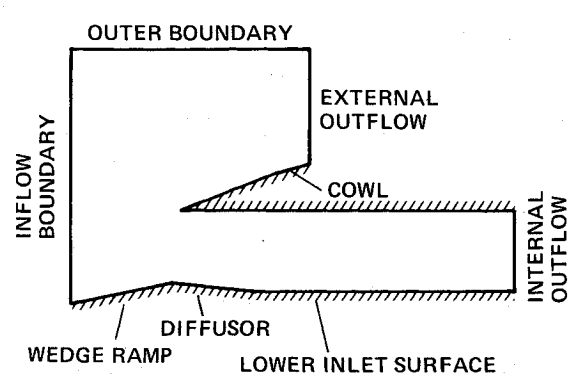

Fig. 1 Surface geometry of inlet.

approach is taken. In this approach, the characteristic compatibility relation, the projection of the momentum equations, and the energy equation are used to calculate the remaining independent variables. The boundary conditions for the subsonic outflow are

$$u^{\text{new}} = u^{\text{old}} + \Delta t f_1, \quad v^{\text{new}} = v^{\text{old}} + \Delta t f_2, \quad \rho^{\text{new}} = \rho^{\text{old}} + \Delta t f_3 \tag{8a}$$

$$p = p_b = \bar{a} + \bar{b}y = \text{const}$$

where

$$f_1 = -(u+c)(\xi_x u_\xi + \eta_x u_\eta) - v(\xi_y u_\xi + \eta_y u_\eta)$$
$$-c(\xi_y v_\xi + \eta_y v_\eta) - \left(\frac{u+c}{\rho c}\right)(\xi_x p_\xi + \eta_x p_\eta) - \bar{b}v$$
$$f_2 = -u(\xi_x v_\xi + \eta_x v_\eta) - v(\xi_y v_\xi + \eta_y v_\eta) - \bar{b}/\rho$$
$$f_3 = -u(\xi_x \rho_\xi + \eta_x \rho_\eta) - v(\xi_y \rho_\xi + \eta_y \rho_\eta) + \bar{b}v \tag{8b}$$

and $\bar{a}$ and $\bar{b}$ are constants allowing for a linear distribution of back pressure across the outflow plane.

At the external outflow boundary, the flow is supersonic and the conservative variables are extrapolated, as is usually the case. The inflow and outer boundaries are placed such that freestream conditions are specified. This completes the specification of the boundaries.

Grid Generation

The transformed equations are somewhat more complicated than the original Cartesian form, but offer several significant advantages. The main advantage is that boundary surfaces in the physical plane can be mapped onto rectangular surfaces in the transformed plane. Another significant aspect of the transformation is that grid points can be concentrated in regions that experience rapid change in the flowfield gradients. This is especially important in the present problem with numerous expansion and compression corners internal and external to the inlet.

To take advantage of the generality of the transformed equations, one needs a fairly automatic method of generating a smoothly varying grid that conforms to arbitrary bodies and allows grid point clustering. The scheme that is chosen for the present application is the Thompson, Thames, and Mastin[12] method which has been altered by Sorenson and Steger[13] and further altered by the present authors. In this method the grid in the physical plane is defined by the solution of a Laplace or a Poisson equation. Grid points are arbitrarily specified on the body boundaries so that even if the Laplace equation is used, the generated grid is not orthogonal. The capability to select the location of boundary node points is one of the desirable features of the scheme and Eqs. (1) and (2) do not assume orthogonality.

Numerical Algorithm

An implicit numerical algorithm is used to solve the equations since in many flowfield problems it is desirable to take a larger time step than that permitted by a conventional explicit scheme. Such a situation may occur if the dependent variables experience a more rapid variation with space than with time. In addition, the unsteady form of the Euler equations [Eq. (1)] were solved to allow for regions of subsonic flow in the inlet to develop if a subcritical or critical flow condition existed.

Conventional Form

The basic numerical algorithm used was developed by Beam and Warming[10] and by Steger.[11] It is second-order accurate in space and time, is noniterative, and is in a spatially factored form referred to as the "delta-form." A fourth-order dissipation term is appended to the right-hand side and in that location helps to control possible numerical instabilities. For either trapezoidal or Euler temporal implicit differencing, the delta form algorithm is given by

$$(I + h\delta_\xi \hat{A}^n - J^{-1}\epsilon_I \nabla_\xi \Delta_\xi J)(I + h\delta_\eta \hat{B}^n - J^{-1}\epsilon_I \nabla_\eta \Delta_\eta J)$$
$$\times (\hat{q}^{n+1} - \hat{q}^n) = -\Delta t(\delta_\xi \hat{E}^n + \delta_\eta \hat{F}^n) - \epsilon_E J^{-1}[(\nabla_\xi \Delta_\xi)^2$$
$$+ (\nabla_\eta \Delta_\eta)^2] J\hat{q}^n = \hat{R}^n \tag{9}$$

where for the convection terms δ_ξ and δ_η are second-order central difference operators, $h = \Delta t$ or $\Delta t/2$ for first- or second-order two-level time differencing, and for convenience the spatial indices are deleted throughout.

The Jacobian matrices $\hat{A}$ an $\hat{B}$ are defined as

$$\hat{A} = \xi_t I + \xi_x A + \xi_y B, \quad \hat{B} = \eta_t I + \eta_x A + \eta_y B \tag{10a}$$

where

$$A = \begin{bmatrix} 0 & 1 & 0 & 0 \\ \frac{(\gamma-3)}{2}u^2 + \frac{(\gamma-1)}{2}v^2 & -(\gamma-3)u & -(\gamma-1)v & (\gamma-1) \\ -uv & v & u & 0 \\ -\gamma u\left(\frac{e}{\rho}\right) + (\gamma-1)u(u^2+v^2) & \gamma\left(\frac{e}{\rho}\right) - \frac{(\gamma-1)}{2}(3u^2+v^2) & -(\gamma-1)uv & \gamma u \end{bmatrix}$$

$$B = \begin{bmatrix} 0 & 0 & 1 & 0 \\ -uv & v & u & 0 \\ \frac{(\gamma-3)}{2}v^2 + \frac{(\gamma-1)}{2}u^2 & -(\gamma-1)u & -(\gamma-3)v & (\gamma-1) \\ -\gamma v\left(\frac{e}{\rho}\right) + (\gamma-1)v(u^2+v^2) & -(\gamma-1)uv & \gamma\left(\frac{e}{\rho}\right) + \frac{(\gamma-1)}{2}(u^2+3v^2) & \gamma v \end{bmatrix} \tag{10b}$$

Numerical dissipation terms are added to the implicit operators, with coefficient ϵ_I, and the explicit side, with coefficient ϵ_E, to control nonlinear instabilities. Typically, $\epsilon_E = 0(h)$ and $\epsilon_I = 2\epsilon_E$.

Diagonal Form

A diagonal form of the implicit algorithm has been developed in Ref. 9. This algorithm retains many of the stability and accuracy characteristics of the original scheme, but requires less computational work. A detailed derivation and analysis of the method can be found in Ref. 9. Here, we shall outline the basic development of the diagonal algorithm.

The standard algorithm is rewritten in inviscid form for convenience as

$$(I+h\delta_\xi \hat{A}^n)(I+h\delta_\eta \hat{B}^n)\Delta q = -\Delta t(\delta_\xi \hat{E}^n + \delta_\eta \hat{F}^n) = \hat{R}^n \tag{11}$$

The similarity transformations which diagonalize A and B (see Warming et al.[16]) are

$$\hat{A} = T_\xi \hat{\Lambda}_\xi T_\xi^{-1}, \quad \hat{B} = T_\eta \hat{\Lambda}_\eta T_\eta^{-1} \tag{12a}$$

where

$$\hat{\Lambda}_\xi = D[U,U,U+c(\xi_x^2+\xi_y^2)^{1/2},\ U-c(\xi_x^2+\xi_y^2)^{1/2}] = \begin{bmatrix} U & 0 & 0 & 0 \\ 0 & U & 0 & 0 \\ 0 & 0 & U+c(\xi_x^2+\xi_y^2)^{1/2} & 0 \\ 0 & 0 & 0 & U-c(\xi_x^2+\xi_y^2)^{1/2} \end{bmatrix} \tag{12b}$$

$$\hat{\Lambda}_\eta = D[V,V,V+c(\eta_x^2+\eta_y^2)^{1/2},\ V-c(\eta_x^2+\eta_y^2)^{1/2}]$$

$$T_k = \begin{bmatrix} 1 & 0 & \alpha & \alpha \\ u & \tilde{k}_y\rho & \alpha(u+\tilde{k}_x c) & \alpha(u-\tilde{k}_x c) \\ v & -\tilde{k}_x\rho & \alpha(v+\tilde{k}_y c) & \alpha(v-\tilde{k}_y c) \\ \dfrac{\phi^2}{(\gamma-1)} & \rho(\tilde{k}_y u-\tilde{k}_x v) & \alpha\left[\dfrac{\phi^2+c^2}{(\gamma-1)}+c\tilde{\theta}\right] & \alpha\left[\dfrac{\phi^2+c^2}{(\gamma-1)}-c\tilde{\theta}\right] \end{bmatrix} \tag{12c}$$

$$T_k^{-1} = \begin{bmatrix} \left(1-\dfrac{\phi^2}{c^2}\right) & (\gamma-1)c^{-2}u & (\gamma-1)c^{-2}v & -(\gamma-1)c^{-2} \\ -\rho^{-1}(\tilde{k}_y u-\tilde{k}_x v) & \tilde{k}_y\rho^{-1} & -\tilde{k}_x\rho^{-1} & 0 \\ \beta(\phi^2-c\tilde{\theta}) & \beta[\tilde{k}_x c-(\gamma-1)u] & \beta[\tilde{k}_y c-(\gamma-1)v] & \beta(\gamma-1) \\ \beta(\phi^2+c\tilde{\theta}) & -\beta[\tilde{k}_x c+(\gamma-1)u] & -\beta[\tilde{k}_y c+(\gamma-1)v] & \beta(\gamma-1) \end{bmatrix}$$

and $\alpha = \rho/(\sqrt{2}c)$, $\beta = 1/(\sqrt{2}\rho c)$, $\tilde{\theta} = \tilde{k}_x u + \tilde{k}_y v$, $\phi^2 = [(\gamma-1)/2](u^2+v^2)$, and, for example, $\tilde{k}_x = k_x/(k_x^2+k_y^2)^{1/2}$.

Relations exist between T_ξ and T_η of the form

$$\hat{N} = T_\xi^{-1} T_\eta, \quad \hat{N}^{-1} = T_\eta^{-1} T_\xi \tag{13}$$

where

$$\hat{N}^j = \begin{bmatrix} 1 & 0 & 0 & 0 \\ 0 & m_1 & -j\mu m_2 & j\mu m_2 \\ 0 & j\mu m_2 & \mu^2(1+m_1) & \mu^2(1-m_1) \\ 0 & -j\mu m_2 & \mu^2(1-m_1) & \mu^2(1+m_1) \end{bmatrix}$$

with $m_1 = (\tilde{\xi}_x\tilde{\eta}_x + \tilde{\xi}_y\tilde{\eta}_y)$, $m_2 = (\tilde{\xi}_x\tilde{\eta}_y - \tilde{\xi}_y\tilde{\eta}_x)$, and $\mu = 1\sqrt{2}$, where $j=1$ for the matrix $\hat{N}$ and $j=-1$ for the inverse matrix $\hat{N}^{-1}$.

Applying the similarity transformations [Eqs. (12) and (13)] to Eq. (11) and factoring T_ξ and T_η out of the spatial operators, we have the diagonal algorithm[10]

$$T_\xi^n(I+h\delta_\xi \hat{\Lambda}_\xi^n)\hat{N}(I+h\delta_\eta \hat{\Lambda}_\eta^n)(T_\eta^{-1})^n \Delta\hat{q} = \hat{R}^n \tag{14}$$

The new implicit operators, $(I+h\delta_\xi \hat{\Lambda}_\xi)$ and $(I+h\delta_\eta \hat{\Lambda}_\eta)$, are still block tridiagonal operators but now the blocks are diagonal in form such that the equations can be reordered into four separate scalar tridiagonal operators. This has a large positive impact on the solution process discussed below.

The solution process for the implicit part of Eq. (14) consists of: 1) $\tilde{S}_1 = (T_\xi^{-1})^n \hat{R}^n$, a matrix-vector multiply at each grid point, since T_ξ^{-1} is known analytically; 2) four scalar tridiagonal inversions for the operator $\tilde{S}_2 = [I+h\delta_\xi \hat{\Lambda}_\xi]^{-1}\tilde{S}_1$; 3) $\tilde{S}_3 = \hat{N}^{-1}\tilde{S}_2$, a matrix-vector multiply at each point; 4) $\tilde{S}_4 = [I+h\delta_\eta \hat{\Lambda}_\eta]^{-1}\tilde{S}_3$, four more scalar tridiagonal inversions; 5) $\Delta\hat{q} = T^n\tilde{S}_4$, another set of matrix-vector multiples; and finally 6) $\hat{q}^{n+1} = \hat{q}^n + \Delta\hat{q}$ to update the solution. This contrasts with the two block tridiagonal inversions required in Eq. (11).

An operation count for the diagonal form of the implicit algorithm yields 233 multiplies, 125 adds, and 26 divides, totaling 384 operations. For the standard algorithm in the transformed coordinates, the operation counts are 410 multiplies, 326 adds, and 10 divides for a total of 746 operations. The use of the diagonal algorithm produces a 33% savings in computer time on a CDC 7600 for a realistic calculation.

Viscous Form

The viscous form of the equations and algorithm has been described in detail by Steger[11] along with a discussion and justification of the "thin-layer" model. In the thin-layer approximation, viscous terms along the body, ξ direction, are neglected and those in the η, or near normal direction, are retained.

The "thin-layer" Navier-Stokes equations in general curvilinear coordinates are

$$\hat{q}_\tau + \hat{E}_\xi + \hat{F}_\eta = Re^{-1}\hat{S}_\eta \tag{15}$$

where

$$\partial_\eta \hat{S} = \partial_\eta J^{-1} \begin{bmatrix} 0 \\ \mu(\eta_x^2+\eta_y^2)u_\eta + (\mu/3)\eta_x(\eta_x u_\eta + \eta_y v_\eta) \\ \mu(\eta_x^2+\eta_y^2)v_\eta + (\mu/3)\eta_y(\eta_x u_\eta + \eta_y v_\eta) \\ \{kPr^{-1}(\gamma-1)^{-1}(\eta_x^2+\eta_y^2)\partial_\eta c^2 \\ \quad +\mu(\eta_x^2+\eta_y^2)(u^2+v^2)_\eta/2 \\ \quad +(\mu/3)(\eta_x u+\eta_y v)(\eta_x u_\eta+\eta_y v_\eta)\} \end{bmatrix}$$

The viscous form of the conventional implicit algorithm is

$$(I+h\delta_\xi \hat{A}^n - \epsilon_I J^{-1}\nabla_\xi\Delta_\xi J)(I+h\delta_\eta \hat{B}^n - \epsilon_I J^{-1}\nabla_\eta\Delta_\eta J - hRe^{-1}\delta_\eta \hat{M}^n)\Delta\hat{q}^n = -\Delta t(\delta_\xi \hat{E}^n + \delta_\eta \hat{F}^n - Re^{-1}\delta_\eta \hat{S}^n) - \epsilon_E J^{-1}[(\nabla_\xi\Delta_\xi)^2 + (\nabla_\eta\Delta_\eta)^2]J\hat{q}^n \tag{16a}$$

where

$$\hat{M} = J^{-1}\begin{bmatrix} 0 & 0 & 0 & 0 \\ m_{21} & \alpha_1\partial_\eta(\rho^{-1}) & \alpha_2\partial_\eta(\rho^{-1}) & 0 \\ m_{31} & \alpha_2\partial_\eta(\rho^{-1}) & \alpha_3\partial_\eta(\rho^{-1}) & 0 \\ m_{41} & m_{42} & m_{43} & m_{44} \end{bmatrix} J$$

$$m_{21} = -\alpha_1\partial_\eta(u/\rho) - \alpha_2\partial_\eta(v/\rho)$$

$$m_{31} = -\alpha_2\partial_\eta(u/\rho) - \alpha_3\partial_\eta(v/\rho)$$

$$m_{41} = \alpha_4\partial_\eta[-(e/\rho^2) + (u^2+v^2)/\rho] - \alpha_1\partial_\eta(u^2/\rho) - 2\alpha_2\partial_\eta(uv/\rho) - \alpha_3\partial_\eta(v^2/\rho)$$

$$m_{42} = -\alpha_4\partial_\eta(u/\rho) - m_{21}$$

$$m_{43} = -\alpha_4\partial_\eta(v/\rho) - m_{31}$$

$$m_{44} = \alpha_4\partial_\eta(\rho^{-1})$$

$$\alpha_1 = \mu[(4/3)\eta_x^2+\eta_y^2], \quad \alpha_2 = (\mu/3)\eta_x\eta_y$$

$$\alpha_3 = \mu[\eta_x^2+(4/3)\eta_y^2], \quad \alpha_4 = \gamma\kappa Pr^{-1}(\eta_x^2+\eta_y^2) \tag{16b}$$

Here Re is the Reynolds number, Pr the Prandtl number, μ the dynamic viscosity, and κ is the coefficient of thermal conductivity.

The inclusion of the viscous term in the second implicit operator of Eq. (16a) makes it difficult to apply the diagonalization to the viscous scheme. This is because the matrix $\hat{M}$ does not have the same eigenvector matrices as B and therefore cannot be simultaneously diagonalized. Tannehill et al.[17] suggest a procedure which will allow us to use the diagonal form. They suggest that the viscous terms in the implicit operators can be neglected for steady-state problems without affecting the stability or accuracy of moderate to high Reynolds number flows. It has been our experience that this can be done as long as a nonzero value of implict dissipation coefficient ϵ_I is used. The elimination of the viscous terms in the implicit operators along with the diagonal algorithm produces a significant reduction in computational cost for steady-state problems.

Results

The results presented here demonstrate that the present numerical technique can calculate complicated two-dimensional inlet flowfields for varying conditions. Also discussed are the advantages of using the diagonal algorithm and of neglecting the implicit viscous term over the use of the standard algorithm. In all cases, the grid is initially calculated by a separate program and is kept nontime varying throughout the calculation.

A two-dimensional cowl-ramp inlet system with a 10 deg ramp and 20 deg wedge-cowl is used as the test case at a freestream Mach number, $M_\infty = 2.0$. Different internal outflow conditions are used to produce supercritical and subcritical flows for inviscid conditions.

A laminar viscous supercritical case is also presented. Since there were no experimental data available, the solution obtained was not optimal with respect to the grid point distribution. The intention here is to demonstrate the ability of the present algorithm to solve viscous as well as inviscid flows. A typical grid system is presented in Fig. 2, where grid lines can be clustered next to the body surfaces either to

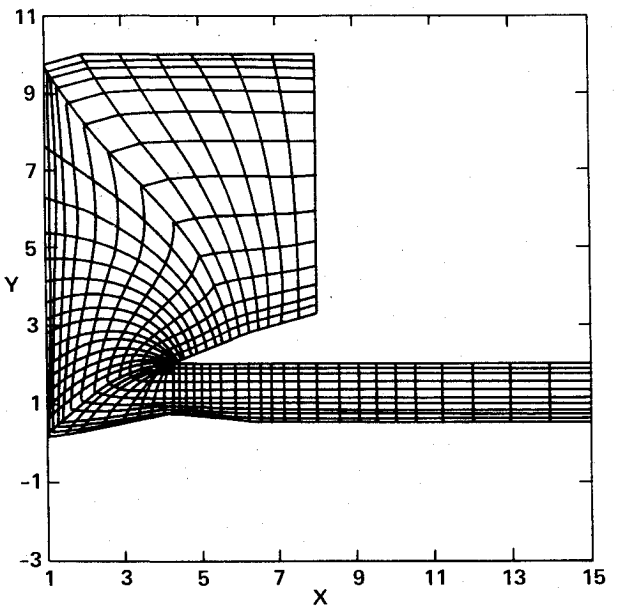

Fig. 2 Grid created by mesh generation program.

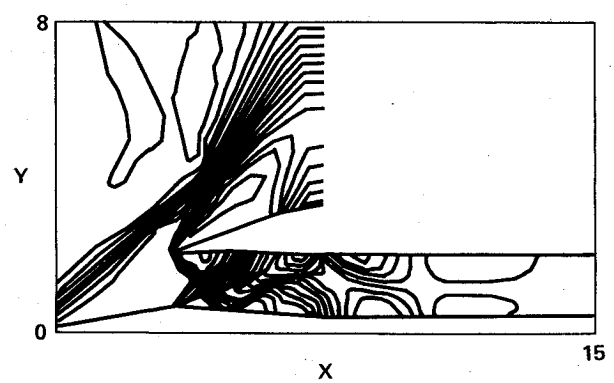

Fig. 3 Density contours for supercritical inviscid flow at $M_\infty = 2.0$.

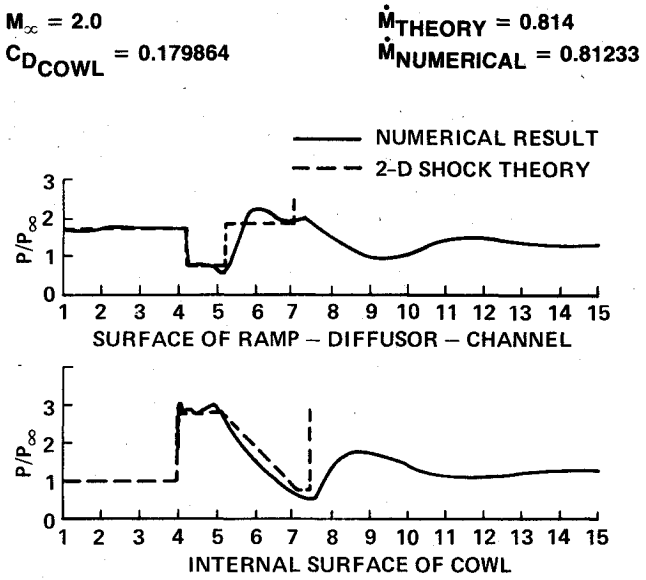

Fig. 4 Comparison between inviscid numerical results and two-dimensional wedge theory.

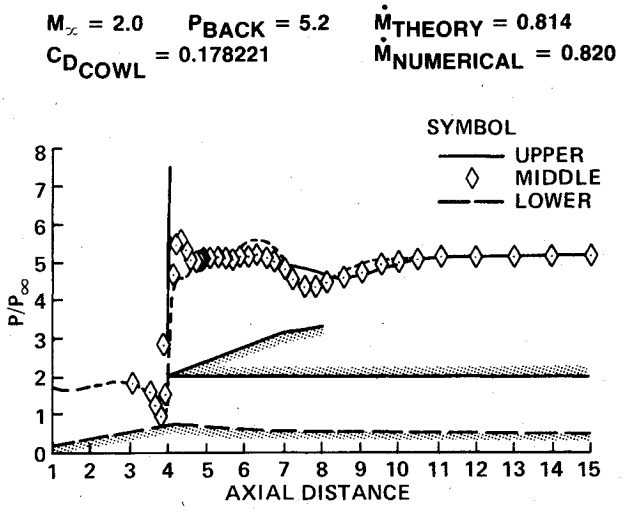

Fig. 5 Pressure variations of subcritical inviscid results showing normal shock wave at the throat.

improve the accuracy of boundary conditions or for viscous resolution.

The numerically generated flowfield as viewed by density contours for a supercritical case is presented in Fig. 3. In the supercritical flow situation, there is supersonic flow throughout the flowfield, causing numerous shock waves and expansion waves which form a complex interaction system within the inlet channel. Figure 4 shows a comparison between the numerical results and the theory for the pressure along the solid surfaces. Since the two-dimensional shock theory does not account for interactions of the waves there are slight differences in the shock locations between the theoretical and numerical solutions.

A subcritical case is presented in Fig. 5 where, based on theoretical calculations, a back pressure of $p/p_\infty = 5.2$ is imposed. Shown are the pressures along the upper and lower surfaces and also along the middle coordinate line of the inlet. A strong shock wave located at the throat is considered to be a product of a critical to subcritical case in near-design conditions. This shock wave developed from a compression wave which formed at the internal outflow plane and then moved upstream. The normal shock wave sits just outside the diffuser throat causing a slight spillage of flow onto the external cowl surface. This increases the cowl drag.

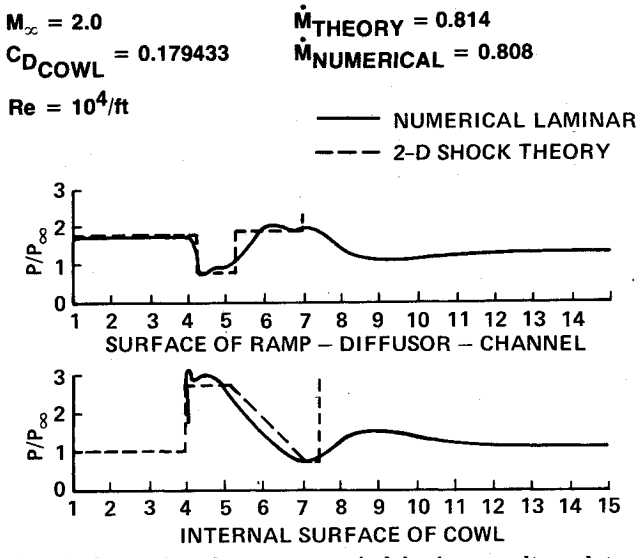

Fig. 6 Comparison between numerical laminar results and two-dimensional wedge theory.

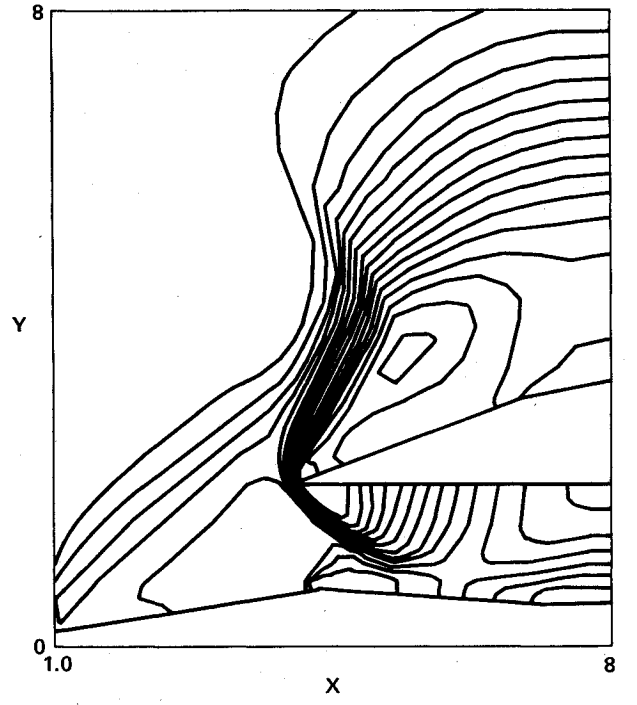

Fig. 7 Pressure contours for supercritical viscous laminar flow, $M_\infty = 2.0$.

A viscous laminar calculation for the supercritical flow conditions at a Re/ft of 10^4 is shown in Figs. 6 and 7. In Fig. 6 the pressure along the inlet surfaces are compared with theory. Even though viscosity dissipates the effects of the shock wave, the overall solution is comparable to the inviscid case. A small reverse flow bubble occurs on the expansion side of the internal wall of the ramp. Pressure contours in the cowl tip region (Fig. 7) show the shock wave that was formed.

The supercritical case shown in Figs. 3, 4, 6, and 7 is used to investigate the effect of the diagonal algorithm, the dropping of the implicit viscous term on the convergence history, and the accuracy and efficiency of the numerical calculations. The conventional algorithm is used as the reference case. All comparisons are for 900 iterations (which assures convergence) and were performed on a CDC 7600 computer for a 66×36 grid point mesh system.

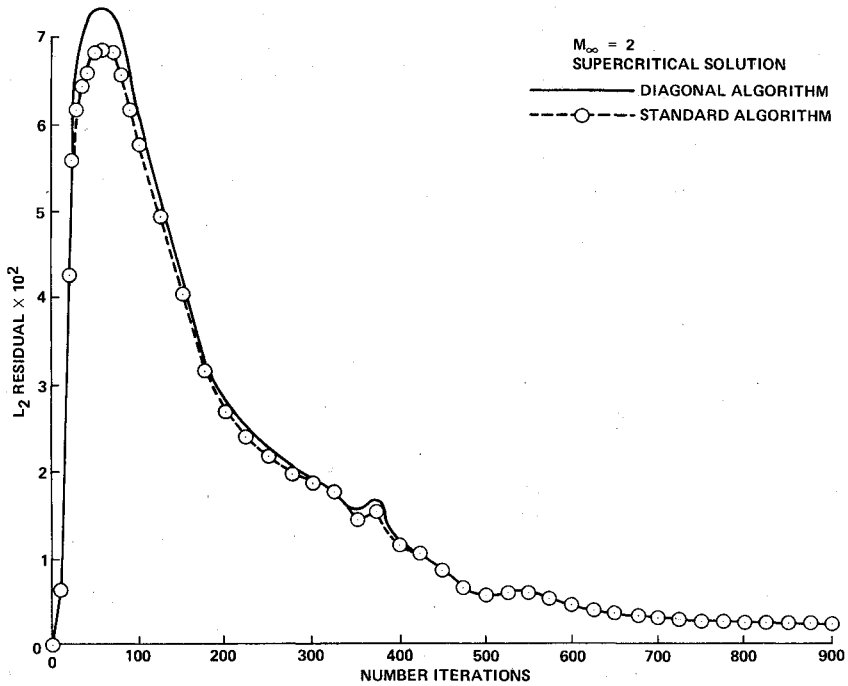

Fig. 8 Convergence history of diagonal algorithm as compared to standard algorithm.

The inviscid calculation using the conventional algorithm requires 794 s of CPU time, whereas the diagonal algorithm requires 522 s, a 34% savings. The convergence history for the two calculations are shown in Fig. 8. The residual is the root mean square of the right-hand side of Eq. (9) and can be considered as the L_2 norm of $\hat{R}^n$. Both cases converge at the same rate and reach identical steady-state solutions.

The viscous calculation requires 975 s of CPU time for the conventional algorithm. By eliminating the viscous term in the implicit operator, the time is reduced to 834 s, a 14.5% reduction. The converged solution is identical to the first solution. Furthermore, combining the viscous approximation with the diagonal algorithm brings the run time down to 567 s, or a 42% reduction over the conventional scheme. In all three cases the convergence history and converged solutions are almost identical.

References

[1] Rizzi, A. W. and Schmidt, W., "Study of Pitot-Type Supersonic Inlet Flowfields Using the Finite-Volume Approach," AIAA Paper 78-115, presented at AIAA 11th Fluid and Plasma Dynamics Conference, Seattle, Wash., July 1978.

[2] Arlinger, B., "Axisymmetric Inlet Flow at Low Supersonic Mach Numbers," *Symposium Transonicum II*, Springer-Verlag, 1975, pp. 200-207.

[3] Reyhner, T. A., "Cartesian Mesh Solution for Axisymmetric Transonic Potential Flow Around Inlets," AIAA Paper 76-421, presented at AIAA 9th Fluid and Plasma Dynamics Conference, San Diego, Calif., July 1976.

[4] Bansod, P., "Supersonic Flow About Ducted Bodies with Subsonic Internal Boundaries," *Journal of Aircraft*, Vol. 12, June 1975, pp. 531-538.

[5] Hawkins, J. E., Kirkland, F. P., and Turner, R. L., "Inlet Spillage Drag Tests and Numerical Flow-Field Analysis at Subsonic and Transonic Speeds of a 1/8-Scale, Two-Dimensional, External-Compression, Variable-Geometry, Supersonic Inlet Configuration," NASA CR-2680, April 1976.

[6] Biringen, S. H., Chaussee, D. S., and McMillan, O. J., "Calculation of Two-Dimensional Inlet Flow Fields by an Implicit Marching Technique," AIAA Paper presented at the AIAA 18th Aerospace Sciences Meeting, Jan. 1980.

[7] Presley, L. L., "Internal Flow Calculations for Axisymmetric Supersonic Inlets at Angle of Attack," AIAA Paper 75-1214, presented at AIAA/SAE 11th Propulsion Conference, Anaheim, Calif., Sept.-Oct. 1975.

[8] Presley, L. L., "A Comparison of a Shock-Capturing Technique with Experimental Data for Three-Dimensional Internal Flows," NASA SP-347, Pt. 1, 1975, pp. 623-642.

[9] Pulliam, T. H. and Chaussee, D. S., "A Diagonal Form of an Implicit Approximation-Factorization Algorithm," *Journal of Computational Physics*, to be published, 1981.

[10] Beam, R. and Warming, R. F., "An Implicit Finite-Difference Algorithm for Hyperbolic Systems in Conservation-Law Form," *Journal of Computational Physics*, Vol. 22, Sept. 1976, pp. 87-110.

[11] Steger, J. L., "Implicit Finite Difference Simulation of Flow About Arbitrary Geometries with Application to Airfoils," AIAA Paper 77-665, presented at AIAA 10th Fluid and Plasma Dynamics Conference, Albuquerque, N. Mex., June 1977.

[12] Thompson, J. F., Thames, F. C., and Mastin, C. M., "Automatic Numerical Generation of Body Fitted Curvilinear Coordinate System for a Field Containing Any Number of Arbitrary Two-Dimensional Bodies," *Journal of Computational Physics*, Vol. 15, 1974, pp. 299-319.

[13] Sorenson, R. and Steger, J. L., "Simplified Clustering of Nonorthogonal Grids Generated by Elliptic Partial Differential Equations," NASA TM X-1977.

[14] Kentzer, C. P., "Discretization of Boundary Conditions on Moving Discontinuities," *Proceedings of the Second International Conference on Numerical Methods in Fluid Dynamics*, Univ. of California, Berkeley, Calif., Sept. 15-19, 1970, pp. 108-113.

[15] Peyret, R. and Viviand, H., "Computation of Viscous Compressible Flows Based on the Navier-Stokes Equations," AGARD-AG-212, 1975.

[16] Warming, R. F., Beam, R. M., and Hyett, B. J., "Diagonalization and Simultaneous Symmetrization of the Gas-Dynamic Matrices," *Mathematical Computation*, Vol. 29, 1975, p. 1037.

[17] Tannehill, J. C., Holst, T. C., and Rakich, J. V., "Numerical Computation of Two-Dimensional Viscous Blunt Body Flows with an Impinging Shock," *AIAA Journal*, Vol. 14, Feb. 1976, pp. 204-211.